npj | climate and atmospheric science

Article

Published in partnership with CECCR at King Abdulaziz University

https://doi.org/10.1038/s41612-024-00688-0

An unusually prolonged Pacific-North American pattern promoted the 2021 winter Quad-State Tornado Outbreaks

Dongmin Kim [1,2] ✉, Sang-Ki Lee [2], Hosmay Lopez [2], Jong-Hoon Jeong [3,4] & Jin-Sil Hong [2,5]

This study examines the large-scale atmosphere-ocean environments that led to the winter tornado outbreak across the Ohio Valley on 10–11 December 2021, also known as the Quad-States Tornado Outbreaks. Here, we show that the Quad-States Tornado Outbreaks occurred under an exceptionally strong and prolonged negative Pacific-North American pattern (PNA), which developed around December 1 and persisted for a month. This unusual PNA produced a strong atmospheric ridge along the south and eastern US seaboard, which in turn helped warm the Gulf of Mexico and produced large-scale environments conducive for tornadogenesis across the Ohio Valley. Further analysis shows that a broad region across the Ohio Valley is particularly vulnerable to extensive winter tornado outbreaks during long-lived negative PNA, whereas a limited region in the central US is exposed to winter tornado activity during short-lived negative PNA. Finally, although the PNA is a mode of internal variability that occurs with or without El Niño—Southern Oscillation, the occurrence of prolonged negative PNA is more frequent during La Niña than during El Niño.

Tornadoes are one of the deadliest and most costly natural disasters in the United States (US). The occurrence of tornadoes increases sharply in boreal spring and then decreases after reaching its peak in April, May, and June. As a result, previous studies have largely focused on warm-season (i.e., boreal spring and summer) US tornado activity[1–12]. However, the occurrence of significant tornadoes (i.e., Enhanced Fujita [EF] scales greater than or equal to two) is not only limited to the warm-season[13–17]. Although relatively rare, winter tornado outbreaks do occur and when they do, they tend to produce disproportionally large socioeconomic impacts on populated US regions, partly due to a lack of societal awareness[16,18].

On December 10, 2021, one of the most destructive winter tornado outbreaks developed in northeastern Arkansas. This tornado outbreak, known as the Quad-State Tornado Outbreaks, struck portions of the Ohio Valley, including Missouri, Illinois, Tennessee, and Kentucky, from December 10 to 11, 2021. According to the National Oceanic and Atmospheric Administration (NOAA; https://www.weather.gov/pah/December-10th-11th-2021-Tornado), the Quad-State Tornado Outbreaks resulted in 66 confirmed tornadoes, 89 fatalities, 672 injuries, and at least $3.9 billion in property damages. The outbreak occurred during a strong multi-year La Niña (i.e., the cold phase of the El Niño—Southern Oscillation, ENSO) and warm sea surface temperature anomalies (SSTAs) were prevalent throughout the Gulf of Mexico (GoM; Fig. 1a). As well-documented in previous studies, both La Niña and warm GoM SSTAs are known to produce favorable large-scale atmospheric conditions for US tornado activity[3,4,13,19,20]. Specifically, La Niña, through extratropical teleconnections, tends to increase the frequency and intensity of winter storm activity over the US, while warm GoM tends to increase the supply of warm and moist low-level air to the US, fueling the winter storms[7,14,15,17,20–22].

Coinciding with the cold tropical Pacific and warm GoM, a strong negative Pacific North American (PNA) pattern developed more than 10 days prior to the Quad-States Tornado Outbreaks and then persisted throughout the event days and beyond until around January 4, 2022 (Fig. 1d). Associated with this unusually prolonged negative PNA, a strong atmospheric ridge developed along the south and eastern US seaboard, increasing the southwesterly low-level wind and the associated flux of warm and moist low-level air from the GoM into the central and eastern US. (Fig. 1b). The increased low-level wind, humidity and near-surface temperature promoted atmospheric instability, evidenced by a strong negative lifted index (LI) and strong low-level wind shear (LLWS) between 1000 and 850 hPa (Fig. 1c), producing highly conducive atmospheric conditions for tornado outbreaks in and around the Mississippi–Ohio Valley. These favorable conditions linked to the prolonged negative PNA pattern also

[1]Cooperative Institute for Marine and Atmospheric Studies, University of Miami, Miami, FL, USA. [2]Atlantic Oceanographic and Meteorological Laboratory, NOAA, Miami, FL, USA. [3]Joint Institute for Regional Earth System Science and Engineering, University of California, Los Angeles, CA, USA. [4]Jet Propulsion Laboratory, California Institute of Technology, Pasadena, CA, USA. [5]Northern Gulf Institute, Mississippi State University, Starkville, MS, USA.
✉e-mail: dongmin.kim@noaa.gov

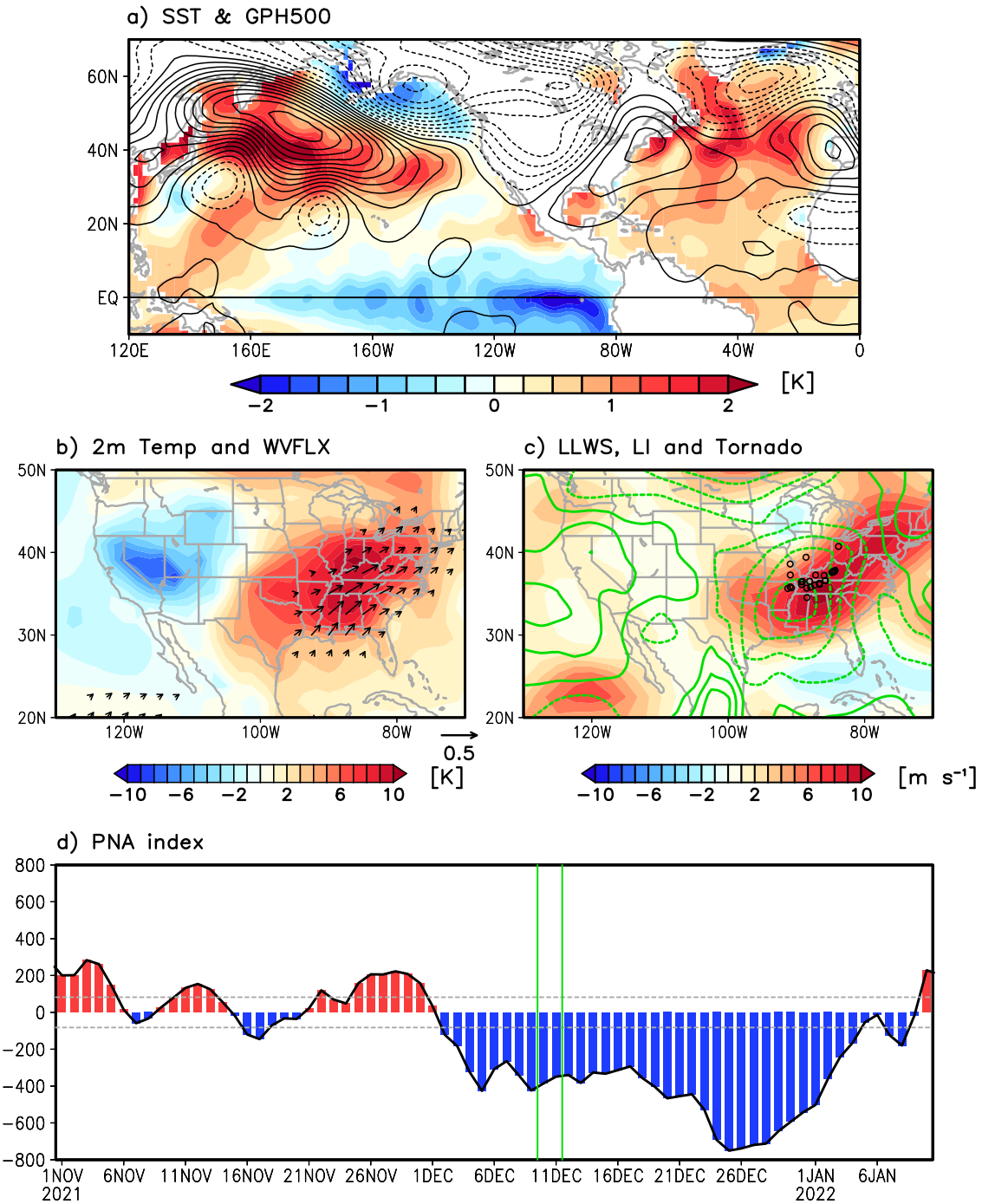

Fig. 1 | Tornado activity and large-scale environments during the Quad-States Tornado Outbreaks on 10-11 December 2021. a Sea surface temperature anomalies (SSTAs, shaded, K) and geopotential height anomalies at 500 hPa (contour, the interval is 50 gpm, solid/dashed lines indicate positive and negative values, respectively) during the Quad-States Tornado Outbreaks (Dec/10–Dec/11/2021). **b** is same as (**a**) but for 2-m air temperature anomalies (shaded, K) and vertically integrated moisture flux anomalies (vectors, kg m^{-1} s^{-1}, omitted below 0.05 kg m^{-1} s^{-1}). **c** is same as (**a**) but for the low-level wind shear between 1000 and 850 hPa (shaded, m s^{-1}), lifted index anomalies (green contours, the interval is 3 K, solid/dashed lines indicate positive and negative values, respectively), and tornadogenesis (black open circles). **d** Time series of daily PNA index from Nov/01/2021 to Jan/10/2022. The black dashed lines are the thresholds of positive and negative PNA events. Green lines represent the period of the Quad-States Tornado Outbreaks (Dec/10–11, 2021).

possibly supported the development of several tornadoes and thunderstorms over Nebraska and Iowa a few days after the Quad-States Tornado Outbreaks (https://www.spc.noaa.gov/climo/reports/211215_rpts.html).

As briefly discussed above, it is very likely that the negative PNA, warm GoM, and La Niña conditions in the Pacific all played sizable roles in fostering the Quad-States Tornado Outbreaks. However, in order to achieve a useful forecast capability for future winter US tornado outbreaks, it is necessary to further investigate large-scale atmospheric and oceanic processes preceding the Quad-States Tornado Outbreaks and other historical winter outbreak events. Since a negative PNA developed more than 10 days prior to the Quad-States Tornado Outbreaks and then persisted for an unusually long period throughout the event days, it is important to address if such a long-lived PNA event is a precursor (or necessary condition) for the development of historical winter US tornado outbreaks. Additionally, given

that SSTAs in the GoM can be forced by surface heat flux anomalies associated with the PNA, it is also important to address if there is any link between the PNA and SSTAs in the GoM. Finally, since negative PNA events occur more frequently during La Niña conditions in the Pacific[23–26], it is useful to further explore if long-lived PNA events are preferred to short-lived ones during La Niña. These key questions are addressed in this study using observational datasets and a fully coupled model simulation.

Results

Impacts of negative PNA and warm GoM on winter US tornado outbreaks

We first carried out a composite analysis to examine the roles of negative PNA and warm GoM in winter US tornado activity. As shown in Fig. 2a, The negative PNA is associated with the development of an anomalous atmospheric ridge around the eastern US. The associated anticyclonic circulation anomalies enhance the low-level southwesterly wind anomalies, increasing the flux of warm and moist low-level air from the GoM to the central and eastern US and LLWS in these regions (Fig. 2b). As a result, near-surface temperature and atmospheric instability (e.g., a decrease in LI) increase over a broad US region in and around Ohio Valley[27,28] (Fig. 2b), thus leading to an increase in winter tornadogenesis in the region (Fig. 2c).

Interestingly, the warm GoM is also linked to a negative PNA-like pattern (Fig. 2d). An atmospheric ridge prevails along the eastern US, similar in location albeit weaker than the negative PNA composite (Fig. 2a), with associated anticyclonic circulation anomalies that enhance the low-level southwesterly wind anomalies. In this case, however, the low-level southwesterly anomalies strengthen predominantly over the southern US; thus, LLWS, the flux of warm and moist low-level air from the GoM, and negative LI are present along the Gulf states (i.e., Texas, Louisiana, Mississippi, and Alabama; Fig. 2e). This suggests that warm GoM is linked to enhanced tornado activity over the southern US and a portion of the southern Ohio Valley (Fig. 2f). To validate the physical relationship between the GoM SSTAs and PNA derived from the observational and reanalysis datasets, we also analyzed the Community Earth System Model Large Ensemble Simulation (CESM-LENS). The composites of SSTAs and geopotential height at 500 hPa derived from CESM-LENS are largely consistent with the results from observations and reanalysis datasets (Supplementary Fig. 1).

Relationship between PNA and GoM SSTAs

The negative PNA-like pattern in the warm GoM composite (Fig. 2d) suggests that GoM SSTAs are linked to the PNA phase. Indeed, it is noted that the GoM is also warm in the negative PNA composite (Fig. 2a). To further examine the relationship between the PNA and GoM SSTAs, we

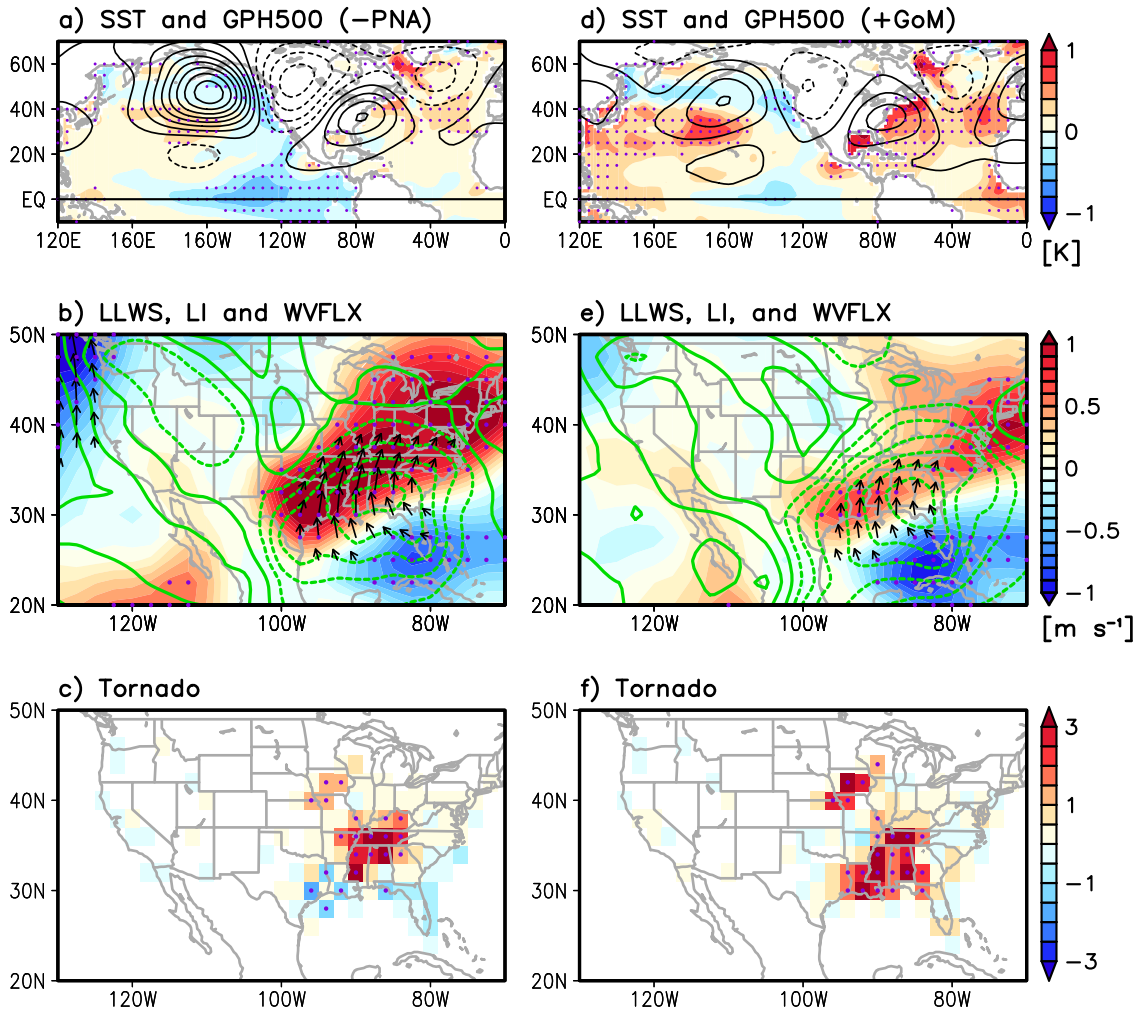

Fig. 2 | Composite analysis of the cold-season US tornado activity and associated large-scale environment during negative PNA and the warm Gulf of Mexico. Composite of **a** SSTAs (shaded, K), geopotential height at 500 hPa (contour, the interval is 20 gpm, solid/dashed lines indicate positive and negative values, respectively), **b** low-level wind shear between 1000 and 850 hPa (shaded, m s^{-1}), the lifted index (green contours, the interval is 3 K, solid/dashed lines indicate positive and negative values, respectively), vertically integrated moisture flux anomalies (vectors, kg m^{-1} s^{-1}, omitted below 0.005), **c** tornadogenesis anomalies (number per November–January season) during negative PNA. **d**–**f** are the same as (**a**–**c**) but for warm Gulf of Mexico SSTAs. Purple dots indicate where correlations are significant above the 95% confidence level based on a two-tailed Student's *t* test.

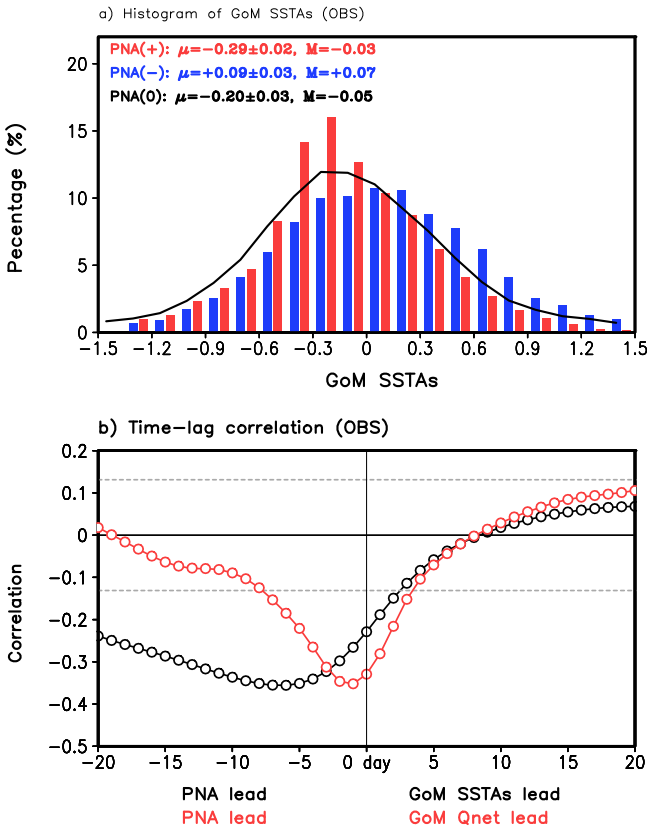

Fig. 3 | Physical links between negative PNA and warm Gulf of Mexico sea surface temperatures. a Histogram of the GoM SSTAs during positive PNA (red bars), negative PNA (blue bars), and neutral case (black line). The mean (μ) plus the 95% significance level and median (M) are shown at the top of the panel. **b** Lead-lag correlation (days) between the PNA index and the GoM SSTAs (black), and between the PNA index and the spatially averaged net surface heat flux (red, positive downward) over the GoM (100°W–80°W, 18°N–31°N). The gray dashed line indicates a 95% significant confidence level based on a Student's t test.

show a histogram of GoM SSTAs during negative, positive, and neutral PNA phases in Fig. 3a. It clearly shows an inverse relationship between the PNA and GoM SSTAs. Specifically, during the negative PNA, the occurrence of warm GoM is more frequent than that during the positive PNA phase. For instance, the probability of extremely warm GoM (>1.2 K) increases by ~300% during the negative PNA compared to that during the positive PNA. During the positive PNA, on the other hand, the occurrence of cold GoM is more frequent than that during the negative PNA. This result supports the hypothesis that GoM SSTAs are physically linked to the PNA phases. The histogram derived from CESM-LENS also supports this result from observational and reanalysis datasets (Supplementary Fig. 2).

To further examine the physical relationship between the PNA and GoM SSTAs, we carried out a lead-lag correlation analysis between the PNA index and GoM SSTAs. As shown in Fig. 3b, the negative PNA leads to warm GoM with a time-lag of approximately 6 days. A consistent result is found from CESM-LENS (Supplementary Fig. 2). The lagged relationship between the PNA and GoM SSTAs is largely due to PNA-induced surface heat flux anomalies over the GoM (Fig. 3b). Further analysis indicates that surface turbulent heat flux (i.e., latent and sensible) anomalies modulated by PNA-induced surface wind speed are the major contributors to the surface heat flux anomalies (Supplementary Fig. 3).

Impact of long- versus short-lived PNA on winter US tornado outbreaks

The lead-lag correlation analysis (Fig. 3b) suggests that if the negative PNA and associated atmospheric ridge over the eastern US persist for 6 days or longer, GoM warms significantly. In contrast, if the negative PNA dissipates within 6 days, GoM SSTAs are not significantly changed. This indicates that long-lived PNA helps warm up the GoM and thus provides a set of ideal environmental conditions for winter US tornado activity. To test this hypothesis, we carried out a composite analysis for the long-lived negative PNA (i.e., exceeding half a standard deviation and persisting for at least 6 days; Supplementary Table 1) versus the short-lived negative PNA (i.e., exceeding half a standard deviation and dissipating in less than 6 days; Supplementary Table 1).

As shown in Fig. 4a, e, 500 hPa geopotential anomalies exhibit a similar spatial pattern during the short- and long-lived negative PNA. However, the associated anomalous ridge over the US eastern seaboard is much more robust during the long-lived PNA. During the short-lived PNA, the atmospheric ridge extends meridionally across the eastern US, producing weak low-level southerly wind anomalies over the central US. This, in turn, increases LLWS, the flux of warm and moist air from the GoM, and decreases LI over the central US, producing favorable conditions for tornadogenesis in this region (Fig. 4b, c). In contrast, during the long-lived PNA, the anomalous ridge is tilted in such a way to produce strong low-level southwesterly anomalies across both the central and eastern US. This increases warm and moist air flux from the GoM and the eastern US coast into the US while increasing LLWS over the eastern US (Fig. 4f). This, in turn, increases atmospheric instability (i.e., a decrease in LI) over the central and eastern US (Fig. 4g). During both the short- and long-lived PNA, surface heat flux is enhanced over the GoM as well as along the eastern US coast (Fig. 4c, g). However, since the reduction of near-surface wind speed is greater during the long-lived negative PNA than during the short-lived negative PNA (Supplementary Fig. 4), the surface flux anomalies are much stronger and more extensive during the long-lived negative PNA (Fig. 4c, g). This explains why the long-lived PNA is more frequently accompanied by warm GoM. These large-scale environmental conditions associated with the short- and long-lived PNA are consistent with those derived from CESM-LENS (Supplementary Fig. 5).

Largely consistent with the large-scale environmental patterns, winter US tornadogenesis is increased over a limited region in the central US (i.e., Arkansas, Missouri, and Illinois) during the short-lived negative PNA (Fig. 4d), while the area of increased winter tornadogenesis is much more extensive across the central and eastern US, including Mississippi, Tennessee, Kentucky, and Indiana, during the long-lived negative PNA (Fig. 4h). Indeed, the area of increased winter tornadogenesis during the long-lived negative PNA is surprisingly consistent with the area affected by the Quad-States Tornado Outbreaks (Fig. 4h).

The role of La Niña in the development of long- and short-lived PNA

Thus far, we have shown that a long-lived negative PNA pattern provides a set of atmosphere and ocean conditions ideal for fostering winter US tornado outbreaks similar to the Quad-States Tornado Outbreaks on 10-11 December 2021. Previous studies have shown that the PNA is a mode of internal variability and thus external forcing (e.g., ENSO) is not required for its development[25,26,29]. However, during La Niña, suppression of deep convection in the tropical Pacific promotes a negative PNA-like pattern through the atmospheric bridge[29–32]. Consequently, cold SSTAs tend to appear in the tropical Pacific during both the short- and long-lived PNA events (Fig. 4a, e).

A related outstanding question is if the 2021–2022 La Niña promoted the unusually prolonged negative PNA event that in turn fostered the Quad-States Tornado Outbreaks. While it is very difficult to find a definitive answer to this question, we may instead explore statistical relationships between the histogram of negative PNA days and ENSO conditions. As expected, the number of negative PNA days in a winter season (i.e., 92 days from November 1 to January 31) increases from 26.4 days per one El Niño season to 33.1 days per one La Niña season (a 25% increase). However, as shown in Fig. 5, the persistence of negative PNA is greater during La Niña than during El Niño. Specifically, about 39 out of 100 negative PNA events are long-lived events (≥6 days) during El Niño conditions, whereas about 52

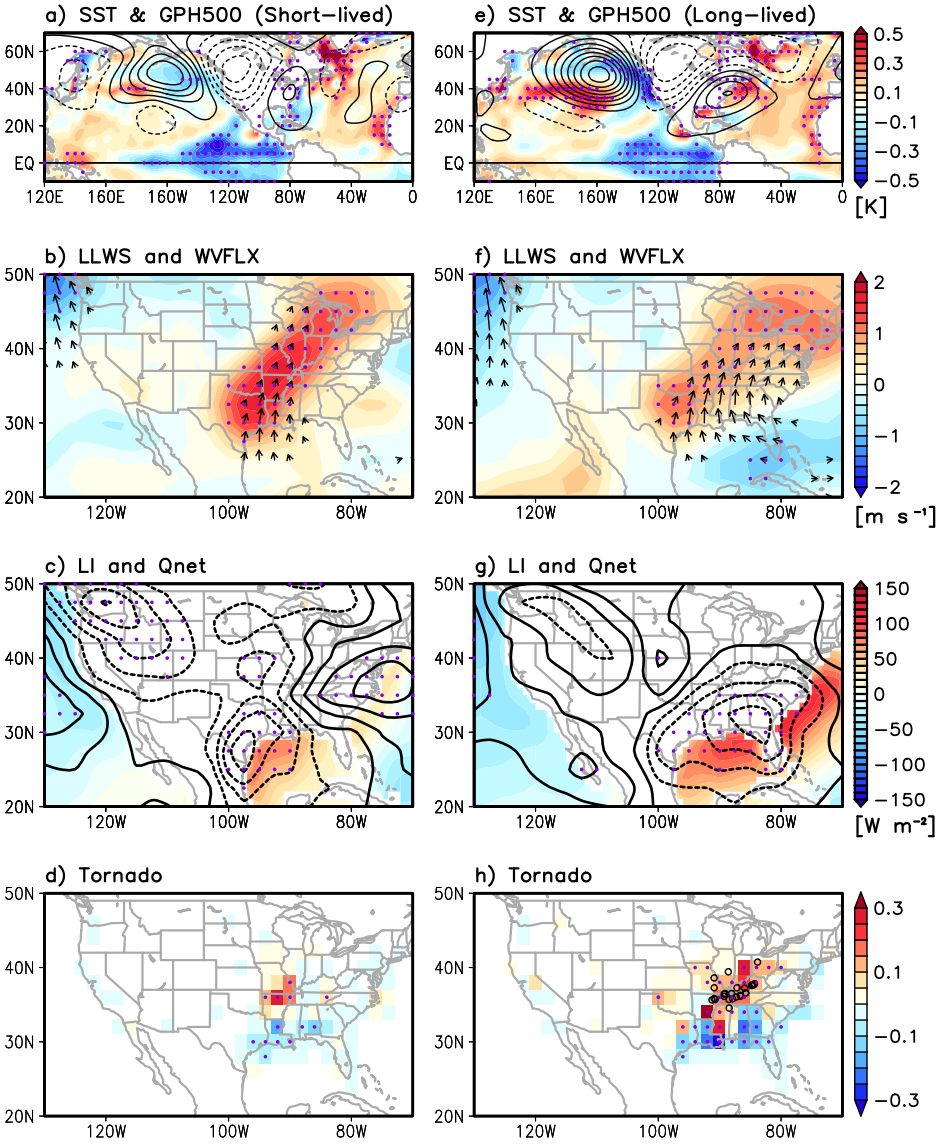

Fig. 4 | Composite analysis of the cold-season US tornado activity and associated large-scale environment during the short-lived negative PNA and the long-lived negative PNA. Composite of **a** SSTAs (shaded, K), geopotential height at 500 hPa (contour, the interval is 20 gpm, solid/dashed lines indicate positive and negative values, respectively), **b** low-level wind shear between 1000 and 850 hPa (shaded, m s^{-1}) and vertically integrated moisture flux anomalies (vectors, kg m^{-1} s^{-1}, omitted below 0.005), **c** net surface flux (shaded, W m^{-2}, positive downward, land area is masked out) and lifted index (black contours, the interval is 3 K; solid/dashed lines indicate positive and negative values, respectively), **d** tornadogenesis anomalies (tornado numbers per a negative PNA event) during the short-lived negative PNA. **e**–**h** are the same as (**a**–**d**) but for during the long-lived negative PNA. Purple dots indicate where correlations are significant above the 95% significant level based on a two-tailed Student's *t* test. Black open circles in (**h**) indicate the tornadogenesis during the Quad-States Tornado Outbreaks.

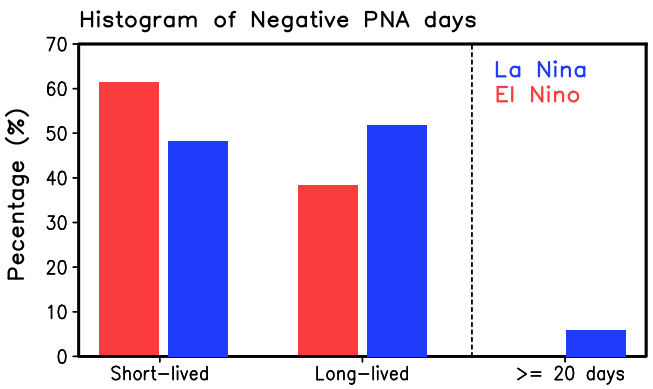

Fig. 5 | Impact of El Niño—Southern Oscillation on the short- and long-lived negative PNA. Histogram of short- and long-lived negative PNA during El Nino (red bars) and La Niña years (blue bars), respectively. The bars at the right side of the dotted line are histograms of extreme long-lived (≥20 days) negative PNA during El Nino (red bar) and La Niña years, respectively.

out of 100 negative PNA events are long-lived events during La Niña conditions. This suggests that long-lived negative PNA events are more prevalent during La Niña conditions than during El Niño conditions. Interestingly, unusually prolonged negative PNA events (≥20 days), as in the case of the Quad-States Tornado Outbreaks, occurred only during La Niña conditions. These results, also supported by the histogram derived from CESM-LENS (Supplementary Fig. 6), suggest that the exceptionally long-lived negative PNA event during December 2, 2021–January 4, 2022 (a total of 34 days) was promoted by the 2021–2022 La Niña.

Discussion

This study shows that the Quad-States Tornado Outbreaks on December 10–11, 2021 is closely tied to the long-lived negative PNA and associated warm GoM that produced a set of highly favorable environmental conditions for a winter tornado outbreak (i.e., increased LLWS and flux of warm and moist air from the GoM, and decreased LI) in and around the Ohio Valley. Further analysis indicates that the long-lived negative PNA produces a robust anomalous atmospheric ridge along the eastern US seaboard, producing anomalous low-level southwesterly wind and flux of warm and

moist low-level air from the GoM into the central and eastern US. Through the associated surface turbulent heat flux, the long-lived negative PNA warms the GoM and thus further enhances the flux of warm and moist low-level air to the US. These atmospheric environments lead to a large increase in atmospheric instability over a broad region of the central and eastern US, increasing the likelihood of tornadogenesis in the region including the Ohio Valley where the Quad-States Tornado Outbreaks predominantly occurred. It is also shown that the occurrence of long-lived negative PNA events is more frequent during La Niña conditions than during El Niño conditions. This supports the idea that the 2021–2022 La Niña promoted the exceptionally long-lived negative PNA event associated with the Quad-States Tornado Outbreaks.

In contrast, the short-lived negative PNA produces a relatively weak and meridionally elongated atmospheric ridge over the eastern US. The atmospheric ridge produces southerly low-level wind anomalies, increasing LLWS and atmospheric instability over the central US. However, due to its short duration, the GoM SSTAs remain relatively neutral. During the short-lived negative PNA, tornadogenesis is increased over the central US. However, due to the relatively weak amplitude of the atmospheric instability (i.e., a decrease in LI) and the near-neutral GoM SSTAs, winter tornadogenesis during the short-lived PNA is increased in a limited region in Arkansas, Missouri, and Illinois.

There remain several questions that are unexplored in this study. First, it is unclear why the Quad-State Tornado Outbreaks occurred only on 10–11 December 2021 despite the persistence of the negative PNA pattern for a month from 1 December 2021. As shown in our analysis, the unusually strong and persistent negative PNA did provide favorable background atmospheric and oceanic states for a severe weather outbreak. However, it is very likely that what actually determined the exact timing of the Quad-State Tornado Outbreaks is synoptic and mesoscale weather dynamics. A negative PNA, La Niña, or warm GoM SSTAs do not necessarily produce a particular synoptic weather pattern. They only provide background environments that may increase the frequency of the weather pattern and the intensity. In addition to this primary factor (i.e., synoptic and mesoscale weather), a positive Arctic Oscillation (AO) developed prior to 1 December, persisted throughout the Quad-States Outbreaks and then transitioned to a neutral phase after 15 December (Supplementary Fig. 7). Thus, the positive AO developed during 1–15 December could be a potential contributing factor based on a positive relationship between the AO and US tornado activity as suggested in previous studies[16,33,34]. Additionally, our study shows that it takes at least 6 days for a negative PNA to persist to significantly warm the GoM. This could be a potential reason why the outbreaks did not occur sooner since the negative PNA developed on 1 December 2021.

Second, it is unclear what triggered the generation of the long-lived negative PNA during the Quad-State Outbreaks. A recent study suggested that Typhoon Nyatoh in the western North Pacific recurved into the mid-latitudes, and then interacted with the extratropical flows to trigger or reinforce the negative PNA pattern; thus, suggesting that the tropical cyclone contributed to the generation of the long-lived negative PNA[35]. Previous studies have also shown that a negative PNA can be forced or triggered by the suppression of tropical Pacific convection (e.g., during La Niña) and associated extratropical Rossby wave propagation[29–31], by transient eddy vorticity fluxes over the extratropics[23,28] and by extraction of kinetic energy from the zonally varying basic state[24,29,31,36–38]. Additionally, an atmospheric ridge over the North Pacific, driven by La Niña conditions, can increase North Pacific SSTAs through anomalous surface turbulent heat fluxes, near-surface mixing, and Ekman currents[39–41]. Recent studies have shown that positive atmosphere-ocean feedback can further enhance the negative PNA-like pattern and warm North Pacific SSTAs[41,42]. Further analysis is required to better understand the potential link between these drivers and the persistence of the PNA.

Another important question is if the frequency of long-lived negative PNA will change in the future. According to several previous studies[43–45], the amplitude of PNA is projected to increase partly due to the increasing variance of SSTAs in the tropical Pacific in the future, while the frequency of PNA is not expected to change significantly. However, it is still unclear whether the duration of the PNA will change in the future climate. Addressing the above questions could potentially help achieve a useful forecast capability for future winter US tornado outbreaks.

Methods

Tornado and reanalysis datasets

The National Centers for Environmental Prediction reanalysis version 1 (NCEP1)[46] is used to derive daily atmospheric variables. Daily SST data is derived from NOAA optimum interpolation SST version 2.1 (OI-SST)[47,48]. The Severe Weather Database (SWD) from NOAA's Storm Prediction Center is used to compute the number of tornadoes. We only counted the tornadoes with the Enhanced Fujita (EF) scale equal to or greater than 1 (EF1–5) to avoid a spurious long-term trend in the tornado dataset[4,12,49]. The study period covers 40 years from 1982 to 2021, focusing on the November–January (NDJ; $n = 3680$) period, or cold season from here onward. To minimize any spurious trend, all data are linearly detrended.

ENSO, PNA and GoM SSTAs

To obtain the indices for ENSO and GoM SSTAs, we used a spatial average of SSTAs over the NINO3.4 region (170°–120°W, 5°S–5°N) and SSTAs over the GoM region (100°W–80°W, 18°N–31°N), respectively. La Niña years are defined as when NDJ seasonal NINO3.4 SSTAs fall below −0.5 K. Warm GoM events are defined as when the daily GoM index is greater than half a standard deviation (i.e., >0.27 K; $n = 802$; Supplementary Table 2). The daily PNA index, following the method used at the NOAA's Climate Prediction Center (CPC), is derived from NCEP1 500 hPa geopotential height anomalies. Negative PNA phases are defined when the daily PNA index falls below half a standard deviation (<−82.18 gpm; $n = 1361$; Supplementary Table 2). The daily AO index is calculated by an empirical orthogonal function of 1000 hPa height anomalies poleward of 20° latitude in the Northern Hemisphere derived from NCEP1 reanalysis, which is the method used at the NOAA's CPC.

CESM-large ensemble simulations

To further test the results derived from the observational and reanalysis datasets, we analyzed a 400-model-year in the Community Earth System Model Large Ensemble Simulation (CESM-LENS) with a constant pre-industrial CO_2 level[50]. All daily indices from CESM-LENS are obtained in the same manner as in the observational and reanalysis datasets. The thresholds for defining warm GoM and negative PNA in the CESM-LENS are 0.18 K ($n = 12{,}260$), and −67.28 gpm ($n = 12{,}401$), respectively (Supplementary Table 2).

Data availability

The National Centers for Environmental Prediction—National Center for Atmospheric Research Reanalysis version 1 (NCEP1) data were downloaded from NOAA's Physical Sciences Laboratory (PSL) at https://psl.noaa.gov/data/gridded/data.ncep.reanalysis.html. NOAA optimum interpolation SST version 2.1 (OI-SST) data were downloaded from NOAA PSL at https://psl.noaa.gov/data/gridded/data.noaa.oisst.v2.highres.html. US tornado reports were downloaded from NOAA's Storm Prediction Center (SPC) at https://www.spc.noaa.gov/wcm/#data. Daily Pacific-North American pattern (PNA) data were downloaded from NOAA's CPC at https://www.cpc.ncep.noaa.gov/products/precip/CWlink/pna/pna.shtml. Daily Arctic Oscillation (AO) data were downloaded from NOAA's CPC at https://www.cpc.ncep.noaa.gov/products/precip/CWlink/daily_ao_index/ao.shtml. CESM-LENS data were downloaded from National Center for Atmospheric Research (NCAR) at https://www.cesm.ucar.edu/community-projects/lens.

Code availability

All statistical analyses were performed using the Grid Analysis and Display System (GrADS), which is publicly available from the Center for Ocean-Land-Atmosphere Studies at http://cola.gmu.edu/grads and NCL, which is

publicly available from the NCAR Command Language (NCL) at https://www.ncl.ucar.edu/. The GrADS, NCL, and Fortran codes used to perform the analyses can be accessed upon request to D.K.

Received: 12 February 2024; Accepted: 9 June 2024;
Published online: 15 June 2024

References

1. Brooks, H. E., Lee, J. W. & Craven, J. P. The spatial distribution of severe thunderstorm and tornado environments from global reanalysis data. *Atmos. Res.* **67**, 73–94 (2003).
2. Tippett, M. K., Sobel, A. H. & Camargo, S. J. Association of U.S. tornado occurrence with monthly environmental parameters. *Geophys. Res. Lett.* **39**, L02801 (2012).
3. Lee, S.-K., Atlas, R., Enfield, D. B., Wang, C. & Liu, H. Is there an optimal ENSO pattern that enhances large-scale atmospheric processes conducive to major tornado outbreaks in the United States? *J. Clim.* **26**, 1626–1642 (2013).
4. Lee, S.-K. et al. U.S. regional tornado outbreaks and their links to ENSO phases and North Atlantic SST variability. *Environ. Res. Lett.* **11**, 044008 (2016).
5. Lee, S.-K., Lopez, H., Kim, D., Wittenberg, A. T. & Kumar, A. A seasonal probabilistic outlook for tornadoes (SPOTter) in the contiguous United States based on the leading patterns of large-scale atmospheric anomalies. *Mon. Weather Rev.* **149**, 901–919 (2021).
6. Jung, E. & Kirtman, B. P. Can we predict seasonal changes in high impact weather in the United States? *Environ. Res. Lett.* **11**, 074018 (2016).
7. Molina, M. J., Timmer, R. P. & Allen, J. T. Importance of the Gulf of Mexico as a climate driver for U.S. severe thunderstorm activity. *Geophys. Res. Lett.* **43**, 12,295–12,304 (2016).
8. Allen, J. T., Molina, M. J. & Gensini, V. A. Modulation of annual cycle of tornadoes by El Niño–Southern Oscillation. *Geophys. Res. Lett.* **45**, 5708–5717 (2018).
9. Baggett, C. F. et al. Skillful subseasonal forecasts of weekly tornado and hail activity using the Madden–Julian Oscillation. *J. Geophys. Res. Atmos.* **123**, 12,661–12,675 (2018).
10. Chu, J. E., Timmermann, A. & Lee, J. Y. North American April tornado occurrences linked to global sea surface temperature anomalies. *Sci. Adv.* **5**, eaaw9950 (2019).
11. Gensini, V. A., Gold, D., Allen, J. T. & Barrett, B. S. Extended U. S. tornado outbreak during late May 2019: a forecast of opportunity. *Geophys. Res. Lett.* **46**, 10,150–10,158 (2019).
12. Kim, D., Lee, S.-K. & Lopez, H. Madden–Julian oscillation–induced suppression of Northeast Pacific convection increases U.S. tornadogenesis. *J. Clim.* **33**, 4927–4939 (2020).
13. Allen, J. T., Tippett, M. K. & Sobel, A. H. Influence of the El Niño/Southern Oscillation on tornado and hail frequency in the United States. *Nat. Geosci.* **8**, 278–283 (2015).
14. Cook, A. R., Leslie, L. M., Parsons, D. B. & Schaefer, J. T. The impact of the El Niño–Southern Oscillation (ENSO) on winter and early spring U.S. tornado outbreaks. *J. Appl. Meteorol. Climatol.* **56**, 2455–2478 (2017).
15. Cook, A. R. & Schaefer, J. T. The relation of El Niño–Southern Oscillation (ENSO) to winter tornado outbreaks. *Mon. Weather Rev.* **136**, 3121–3137 (2008).
16. Childs, S. J., Schumacher, R. S. & Allen, J. T. Cold-season tornadoes: climatological and meteorological insights. *Weather Forecast.* **33**, 671–691 (2018).
17. Molina, M. J., Allen, J. T. & Gensini, V. A. The Gulf of Mexico and ENSO influence on subseasonal and seasonal CONUS winter tornado variability. *J. Appl. Meteorol. Climatol.* **57**, 2439–2463 (2018).
18. Childs, S. J. & Schumacher, R. S. Cold-season tornado risk communication: case studies from November 2016 to February 2017. *Weather Clim. Soc.* **10**, 419–433 (2018).
19. Wang, H., Kumar, A., Diawara, A., DeWitt, D. & Gottschalck, J. Dynamical–statistical prediction of week-2 severe weather for the United States. *Weather Forecast.* **36**, 109–125 (2021).
20. Molina, M. J., Allen, J. T. & Prein, A. F. Moisture attribution and sensitivity analysis of a winter tornado outbreak. *Weather Forecast.* **35**, 1263–1288 (2020).
21. Weiss, S. J. Some aspects of forecasting severe thunderstorms during cool-season return-flow episodes. *J. Appl. Meteorol.* **31**, 964–982 (1992).
22. Molina, M. J. & Allen, J. T. On the moisture origins of tornadic thunderstorms. *J. Clim.* **32**, 4321–4346 (2019).
23. Feldstein, S. B. The timescale, power spectra, and climate noise properties of teleconnection patterns. *J. Clim.* **13**, 4430–4440 (2000).
24. Feldstein, S. B. Fundamental mechanisms of the growth and decay of the PNA teleconnection pattern. *Quart. J. R. Meteorol. Soc.* **128**, 775–796 (2002).
25. Lopez, H. & Kirtman, B. P. ENSO influence over the Pacific North American sector: uncertainty due to atmospheric internal variability. *Clim. Dyn.* **52**, 6149–6172 (2019).
26. Li, X., Hu, Z., Liang, P. & Zhu, J. Contrastive influence of ENSO and PNA on variability and predictability of North American winter precipitation. *J. Clim.* **32**, 6271–6284 (2019).
27. Leathers, D. J., Yarnal, B. & Palecki, M. A. The Pacific/North American teleconnection pattern and United States climate. Part I: regional temperature and precipitation associations. *J. Clim.* **4**, 517–528 (1991).
28. Franzke, C., Feldstein, S. B. & Lee, S. Synoptic analysis of the Pacific–North American teleconnection pattern. *Quart. J. R. Meteorol. Soc.* **137**, 329–346 (2011).
29. Dai, Y., Feldstein, S. B., Tan, B. & Lee, S. Formation mechanisms of the Pacific–North American teleconnection with and without its canonical tropical convection pattern. *J. Clim.* **30**, 3139–3155 (2017).
30. Horel, J. D. & Wallace, J. M. Planetary-scale atmospheric phenomena associated with the Southern Oscillation. *Mon. Weather Rev.* **109**, 813–829 (1981).
31. Mori, M. & Watanabe, M. The growth and triggering mechanisms of the PNA: a MJO-PNA coherence. *J. Meteorol. Soc. Jpn.* **86**, 213–236 (2008).
32. Clark, J. P. & Feldstein, S. B. The temperature anomaly pattern of the Pacific–North American teleconnection: growth and decay. *J. Atmos. Sci.* **79**, 1237–1252 (2022).
33. Brown, M. C. & Nowotarski, C. J. Southeastern US tornado outbreak likelihood using daily climate indices. *J. Clim.* **33**, 3229–3252 (2020).
34. Tippett, M. K., Lepore, C. & L'Heureux, M. L. Predictability of a tornado environment index from El Niño–Southern Oscillation (ENSO) and the Arctic Oscillation. *Weather Clim. Dyn.* **3**, 1063–1075 (2022).
35. Jiang, N., Liu, B., Zhu, C. & Chen, Y. Remote linkage of record breaking U.S. tornado outbreaks to the tropical cyclone in the western North Pacific in December 2021. *Environ. Res. Lett.* **18**, 044036 (2023).
36. Simmons, A. J., Wallace, J. & Branstator, G. W. Barotropic wave propagation and instability, and atmospheric teleconnection patterns. *J. Atmos. Sci.* **40**, 1363–1392 (1983).
37. Branstator, G. Low-frequency patterns induced by stationary waves. *J. Atmos. Sci.* **47**, 629–649 (1990).
38. Branstator, G. The maintenance of low-frequency atmospheric anomalies. *J. Atmos. Sci.* **49**, 1924–1946 (1992).
39. Alexander, M. A. & Scott, J. D. The role of Ekman ocean heat transport in the Northern Hemisphere response to ENSO. *J. Clim.* **21**, 5688–5707 (2008).
40. Alexander, M. A. et al. The atmospheric bridge: the influence of ENSO teleconnections on air–sea interaction over the global oceans. *J. Clim.* **15**, 2205–2231 (2002).
41. Larson, S. M., Okumura, Y., Bellomo, K. & Breeden, M. L. Destructive interference of ENSO on North Pacific SST and North American

precipitation associated with Aleutian low variability. *J. Clim.* **35**, 3567–3585 (2022).
42. Mori, M. et al. Northern Hemisphere winter atmospheric teleconnections are intensified by extratropical ocean-atmosphere coupling. *Commun. Earth Environ.* **5**, 124 (2024).
43. Chen, Z., Gan, B., Wu, L. & Jia, F. Pacific-North American teleconnection and North Pacific Oscillation: historical simulation and future projection in CMIP5 models. *Clim. Dyn.* **50**, 4379–4403 (2018).
44. Chen, Z. et al. The influence of Pacific-North American teleconnection on the North Pacific SST anomalies in Wintertime under the global warming. *Clim. Dyn.* **60**, 1481–1494 (2023).
45. Coburn, J. & Pryor, S. C. Evolution of the internal climate modes under future warming. *J. Clim.* **36**, 511–529 (2023).
46. Kalnay, E. et al. The NCEP/NCAR 40-year reanalysis project. *Bull. Am. Meteorol. Soc.* **77**, 437–472 (1996).
47. Reynolds, R. W. et al. Daily high-resolution-blended analyses for sea surface temperature. *J. Clim.* **20**, 5473–5496 (2007).
48. Huang, B. et al. Improvements of the Daily Optimum Interpolation Sea Surface Temperature (DOISST) Version 2.1. *J. Clim.* **34**, 2923–2939 (2021).
49. Verbout, S. M., Brooks, H. E., Leslie, L. M. & Schultz, D. M. Evolution of the U.S. tornado database: 1954–2003. *Weather Forecast.* **21**, 86–93 (2006).
50. Kay, J. E. et al. The Community Earth System Model (CESM) Large Ensemble Project: a community resource for studying climate change in the presence of internal climate variability. *Bull. Am. Meteorol. Soc.* **96**, 1333–1349 (2015).

Acknowledgements

The authors thank Breanna Zavadoff for helpful comments and suggestions. This work was carried out under the auspices of the Cooperative Institute for Marine and Atmospheric Studies (CIMAS), a cooperative institute of the University of Miami, and NOAA, cooperative agreement NA20OAR4320472, and supported by NOAA's Oceanic and Atmospheric Research and NOAA's Atlantic Oceanographic and Meteorological Laboratory. H.L. and S.-K.L. acknowledge support from base funds from AOML's Physical Oceanography Division.

Author contributions

D.K. and S.-K.L. conceived the study, D.K. performed the analysis and wrote the initial draft of the paper. All authors significantly contributed to the discussion and interpretation of results and reviewed the paper.

Competing interests

The authors declare no competing interests.

Additional information

Supplementary information The online version contains supplementary material available at https://doi.org/10.1038/s41612-024-00688-0.

Correspondence and requests for materials should be addressed to Dongmin Kim.